Proc. 2nd Saudi Sci. Conf.,Fac. Sci., KAU, 15-17 March 2004, ***Part II,*** pp. 159-170 (2005 A.D./1425 A.H.)

Operation Stability of Semiconductor Lasers In Optical Fiber Communication Systems

MOUSTAFA F. AHMED and SAFWAT W.Z. MAHMOUD
Department of Physics, Faculty of Science, Minia University, 61519 El-Minia, Egypt
Email: m.farghal@link.net

ABSTRACT. The paper reports on analysis of the dynamics and operation stability of pumping semiconductor lasers of optical fiber amplifiers in optical communication systems. The parameters of the amplifier system that correspond to stable operation and low intensity noise are explored. The study is based on a time-delay model of the rate equations of the photon number, optical phase and the injected electron number. The analyses are performed in terms of the instantaneous fluctuations of the laser intensity, the corresponding bifurcation diagram and phase portraits, and the relative intensity noise. The frequency spectra of the intensity noise under strong feedback are characterized. The results indicate that the laser stability improves when the length of the external cavity formed between the laser and a fiber grating decreases where the laser operates almost in either pulsation or continuous wave. The operation becomes almost chaotic interrupted by narrow regions of continuous wave in the extreme of long external cavities, which degrades the laser stability.

1. Introduction

Optical fiber amplifiers have been recently utilized to compensate weakness of the transmitted signal down optical fibers and hence to increase the transmission distance in optical fiber communication systems (Agrawal, 2003). In such systems, semiconductors lasers consisting with external fiber cavities terminated with fiber gratings (FGs), as shown in Fig. 1, have been popularly used as exciting sources for fiber amplifiers (rare-earth-element doped fibers). The external fiber cavity is introdueed to increase the lasing power over both the internal (the solitary laser) and the external fiber eavities. The FG is introduced to lock the lasing frequency to a single frequency of the external cavity resonanees or to a limited range of frequencies. The pumping semiconductor lasers are designed with an antireflection-coated front facet. Therefore, these lasers suffer from very strong external optical feedback (OFB) due to reflection of the laser light by the FG and re-injection into the laser cavity (Mokai & Otsuka, 1985). Recent investigations of the operation characteristics of such lasers have indicated that the device may operate in continuous wave (CW) or pulsation (periodic or quasi-periodic) depending on the lasing conditions and the system configuration (Abdulrhmann *et al.*, 2003). One drawback of the optical fiber amplifier is that it amplifies both the signal and the noise induced upon propagation of the lightwave down the fibers. Stabilizing the operation of the pumping

laser and suppressing the corresponding intensity noise to its lowest quantum level are necessary to improve the performance of the optical amplifier systems. Therefore, characterization of the intensity noise is prerequisite in this regard.

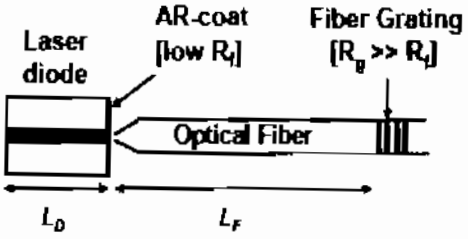

Fig. (1). Scheme of a pumping laser diode in an optical fiber amplifier system.

Recently, a new model of OFB in semiconductor laser diodes has been reported which is exceptionally applicable to an arbitrary strength of the OFB (Abdulrhmann *et al.*, 2003). In this paper, we apply such a model to analyze the dynamics, intensity noise, and operation stability of pumping lasers in fiber amplifier systems. We are aimed at exploring the OFB parameters that correspond to stable operation and low noise, namely, the reflectivity of the FG and its distance to the pumping laser. The analyses are made in terms of the instantaneous fluctuations of the light intensity, the corresponding bifurcation diagram and phase portrait, and the spectrum of the relative intensity noise (RIN).

The paper is structured as follows. The theoretical model of laser dynamics and noise is given in the next section. Section 3 presents the procedures of applying the proposed model in numerical calculations. In section 4, we demonstrate the simulation results of laser dynamics and noise under OFB. The conclusions are given in section 5.

2. Theoretical Model

The proposed model of laser operation under OFB in a fiber amplifier system is schematically illustrated in Fig. 2. The light emitted from the laser front facet at a time t travels for a time of $\tau = 2n_F L_F/c$ in the external cavity formed between the laser front facet of reflectivity R_f and the FG of reflectivity R_g , with L_F and n_F as the length and refractive index of the external cavity, and c as the speed of light in vacuum. The light then travels back to the cavity and re-injects into the laser cavity through the front facet. That is, at a time t and at the front facet, the photon number $S(t)$ inside the cavity $S(t)$ is influenced by the time-delayed value $S(t-\tau)$ in the external cavity. Such phenomenon is described by the following rate equations of the photon number $S(t)$, optical phase $\theta(t)$ and injected electron number $N(t)$ (Abdulrhmann *et al.*, 2003):

$$\frac{dS}{dt} = \left(A - BS - G_{th0} + \frac{c}{n_D L_D} \ln|U| \right) S + \frac{a\xi}{V} N + F_S(t), \tag{1}$$

$$\frac{d\theta}{dt} = \frac{1}{2}\left[\frac{\alpha a \xi}{V}\left(N - \bar{N}\right) - \frac{c}{n_D L_D}\varphi \right] + F_\theta(t), \tag{2}$$

$$\frac{dN}{dt} = -AS - \frac{N}{\tau_s} + \frac{I}{e} + F_N(t), \tag{3}$$

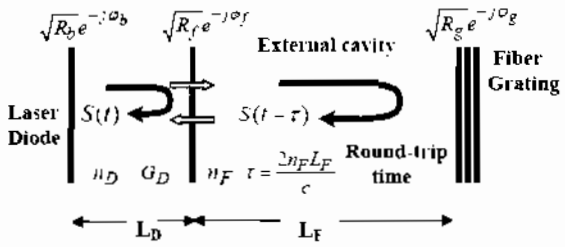

Fig. (2). Scheme of a laser diode under OFB in an optical communication system.

where A and B are linear and nonlinear coefficients of optical gain G_D, respectively. They are determined in terms of the number of injected electrons N as (Ahmed & Yamada, 1998),

$$A = \frac{a\xi}{V}\left(N - N_g\right), \tag{4}$$

$$B = \frac{9\pi c}{2\varepsilon_0 n_r^2 \hbar\lambda}\left(\frac{\xi\tau_{in}}{V}\right)^2 a\left|R_{cv}\right|^2\left(N - N_s\right). \tag{5}$$

The parameters in the above equations are defined as follows. a is a tangential coefficient of A, ξ is the field confinement factor in the active region, V, L_D, and n_D are the volume, length and spatially-averaged refractive index of the active region, respectively, N_g is the electron number at transparency, N_s is an electron number characterizing the nonlinear gain coefficient, $\bar{N}$ is a time-averaged value of N, λ is the emission wavelength, $|Rcv|^2$ is the squared absolute value of the dipole moment, G_{th0} is the threshold gain in the solitary laser, α is the linewidth enhancement factor, I is the injection current, τ_s is the lifetime of electrons due to spontaneous emission, τ_{in} is the intraband relaxation time, and e is the electron charge. The term $a\xi N/V$ in Eq. (1) indicates the rate of inclusion of the spontaneous emission into the lasing mode.

The OFB is counted in terms of the function U and its argument φ which are defined in terms of the delay round-trip time τ as (Abdulrhmaun *et al.*, 2003):

$$\begin{aligned} U &= 1 - K_{ex}\,\exp\{-j\psi\}\sqrt{\frac{S(t-\tau)}{S(t)}}\,\exp\left\{j\left(\theta(t-\tau)-\theta(t)\right)\right\}, \\ &= |U|\,\exp\{-j\varphi\} \end{aligned} \tag{6}$$

ψ represents the phase difference between the delayed injected field and the reflected field to the laser cavity at the front facet,

$$\psi = \omega\tau + \varphi_f + \varphi_g, \tag{7}$$

where φ_f and φ_g are the phase changes of the field at the front facet and the fiber grating, respectively, and $\omega\tau$ is the phase delay during each round trip in the external cavity. The feedback coefficient K_{ex} measures the strength of OFB and is determined by the ratio of the external reflectivity R_g to the front-facet reflectivity R_f as,

$$K_{ex} = \left(1 - R_f\right)\sqrt{\frac{\eta R_g}{R_f}}, \tag{8}$$

where η is the coupling ratio of the externally reflected light into the laser cavity. The argument φ of the feedback function U is obviously given by:

$$\varphi = -\tan^{-1}\left\{\frac{\mathrm{Im}[U]}{\mathrm{Re}[U]}\right\} + m\pi, \tag{9}$$

where m is an integer. Determining the value of φ in the two-dimensional space (Re[U]-Im[U]) depends on both the signs and magnitudes of Re[U] and Im[U].

The terms $F_S(t)$, $F_\theta(t)$ and $F_N(t)$ are Langevin noise sources of a Gaussian type with zero means, and satisfy the following cross-correlations (Ahmed *et al.*, 2001):

$$F_a(t)\,F_b(t') = V_{ab}\,\delta(t - t'), \tag{10}$$

where a and b stand for any of S, N or θ. These random terms are added to the rate equations to account for the quantum noises associated with inclusion of the spontaneous emission and recombination processes of charge carriers (Ahmed *et al.*, 2001). The variances V_{ab} are determined from the steady-state solutions $\bar{S}$ and $\bar{N}$ of Eqs. (1)-(3).

The noise content of the output fluctuations is determined in terms of the RIN. The RIN is calculated from the fluctuations $\delta S(t) = S(t) - \bar{S}$ of $S(t)$ via the equation (Ahmed *et al.* 2001):

$$RIN = \frac{1}{\bar{S}^2}\left\{\frac{1}{T}\left|\int_0^T \delta S(\tau) e^{-j\Omega\tau} d\tau\right|^2\right\}, \tag{11}$$

where Ω is the Fourier frequency and $\bar{S}$ is the time-average value of $S(t)$.

3. Numerical Calculations and Results

3.1. Procedures of Calculations

In the present calculations, typical values of the parameters of both 980 nm InGaAs laser diodes and the geometry of fiber amplifier systems are employed. These values are listed in Table 1. The rate equations (1)-(3) are solved numerically by means of the fourth-order Runge-Kutta method. The time step of integration is set as short as Δt = 5ps to guarantee fine resolution of the OFB-induced dynamics. This small time step Δt corresponds to a cut-off frequency much higher than the external-cavity mode-separation frequency $f_{ex} = 1/\tau$. The operation state is examined in the period t = 8~10 μs during which the operation state is fixed. The integration is first made without OFB (case of the solitary laser) from time t=0 until the round trip time τ. The calculated values of $S(t{:}0 \rightarrow \tau)$ and $\theta(t{:}0 \rightarrow \tau)$ are then stored for use as time delayed values $S(t-\tau)$ and $\theta(t-\tau)$ for further integration of the rate equations including OFB terms. The phase difference ψ is arbitrary and is set as zero in the present calculations. The spectrum of the RIN is computed directly from the obtained instantaneous values of $\delta S(t_i) = S(t_i) - \bar{S}$ by applying the fast Fourier transform (FFT) to integrate the discrete version of Eq. (11) as (Ahmed, 2003):

$$RIN \equiv \frac{1}{\bar{S}^2}\frac{\Delta t^2}{T}\left|FFT\left[\delta S(t_i)\right]\right|^2, \tag{12}$$

Table (1). Typical Values of Parameters of Algaas Lasers and Geometry of Optical-Fiber Amplifier Systems.

Symbol	Parameter	Value	Unit
L_f	Distance of laser diode to optical disc	varies	Cm
n_f	Refractive index of the fiber	1.5	--
a	Tangential parameter of linear gain	$2.21\text{x}10^{-12}$	m^3s^{-1}
Ng_2	Electron number at transparency	$4.08\text{x}10^{8}$	--
R_{cv}	Square value of the dipole moment	$2.8\text{x}10^{-57}$	C^2m^2
N_s	Value of the electron number Characterizing the nonlinear gain	$1.53\text{x}10^{8}$	--
τ_{in}	Intraband relaxation time	0.1	ps
τ_s	Electron lifetime	2.79	ns
α	Linewidth enhancement factor	2	--
n_D	Refractive index of active region	3.5	--
L_D	Length of the active region	800	μm
V	Volume of the active region	400	μm^3
ξ	Field confinement factor	0.1	--
R_f	Reflectivity at front facet	0.02	--
R_b	Reflectivity at back facet	0.98	--

In order to perform the above calculations, discrete generations of the noise sources at each instant are necessary. Theses processes require enough care in order to satisfy the cross-correlations of the noise source $F_N(t_i)$ with $F_S(t_i)$ and $F_\theta(t_i)$ at each time t_i, which originate in the cross-correlation between S and N during the lasing action. In this paper, we follow the self-consistent techniqc proposed by Ahmed et al. (Ahmed *et al.*, 2001) to adopt such generation processes. The obtained forms of the noise sources are:

$$F_S(t_i) = \sqrt{\frac{V_{SS}(t_i)}{\Delta t}}\, g_S \tag{13}$$

$$F_\theta(t_i) = \frac{1}{S(t_i - 1) + 1}\sqrt{\frac{V_{SS}(t_i)}{\Delta t}}\, g_\theta \tag{14}$$

$$F_N(t_i) = \sqrt{\frac{V_{NN}(t_i) + 2k_S(t_i)V_{NS}(t_i)}{\Delta t}}\, g_N - k_S(t_i)\left\{F_S(t_i) + 2\left[S(t_{i-1}) + 1\right]F_\theta(t_i)\right\} \tag{15}$$

with

$$V_{SS}(t_i) = 2\frac{a\xi}{V}\left[S(t_{i-1}) + 1\right]N(t_{i-1}) \tag{16}$$

$$V_{NN}(t_i) = 2\left[\frac{1}{\tau_s} + \frac{a\xi}{V}S(t_{i-1})\right]N(t_{i-1}) \tag{17}$$

$$V_{NS}(t_i) = -\frac{a\xi}{V}N(t_{i-1})\left[S(t_{i-1}) + 1\right] + N_g S(t_{i-1}) \tag{18}$$

$$k_S(t_i) = -\frac{V_{NS}(t_i)}{V_{SS}(t_i)} \quad . \tag{19}$$

In the above equations, g_S, $g\theta$, and g_N are three independent Gaussian random numbers with means of zero and variances of unity. They are obtained at each integration step by applying the Box-Mueller approximation (Press *et al.*, 1992) to a set of three uniformly distributed independent random numbers generated by the computer.

4. Results and Discussion

4.1. Time variation of laser intensity and spectrum of RIN

Examples of the simulation results of laser output and noise in the strong OFB regime are given in Fig. 3 when the injection current is well above the threshold, $I=5I_{th0}$ with I_{th0} as the threshold current in the solitary laser. Figures 3(a)-(c) plot the temporal trajectories of the photon number $S(t)$ when K_{ex}=1.1, 3.9 and 4.4, respectively. Figures 3(d)-(f) plot the corresponding phase portraits [$S(t)$ versus $N(t)$], and Figs. 3(g)-(i) plot the corresponding spectra of the RIN. Figure 3(a) shows that the emitted photon number $S(t)$ fluctuates around its average value $\bar{S}$. The amplitude of the fluctuations is comparable to that of the solitary laser. That is, the laser operates in CW. Figure 3(d) indicates almost a point attractor of the phase portrait. The corresponding RIN spectrum shown in Fig. 3(g) exhibits low-frequency components little higher than the components of the RIN of the solitary laser. The spectrum has peaks around the sub-harmonic 1/2 of the compound-cavity mode-separation frequency $f_c=c/2(n_DL_D+n_{ex}L_{ex}) \approx$ 4GHz and its higher harmonics. This indicates that the fluctuations of $S(t)$ have a periodic component with $f_c/2$. The peak of the RIN of the solitary laser corresponds to the well-known relaxation oscillation of frequency $f_r \approx 4$ GHz.

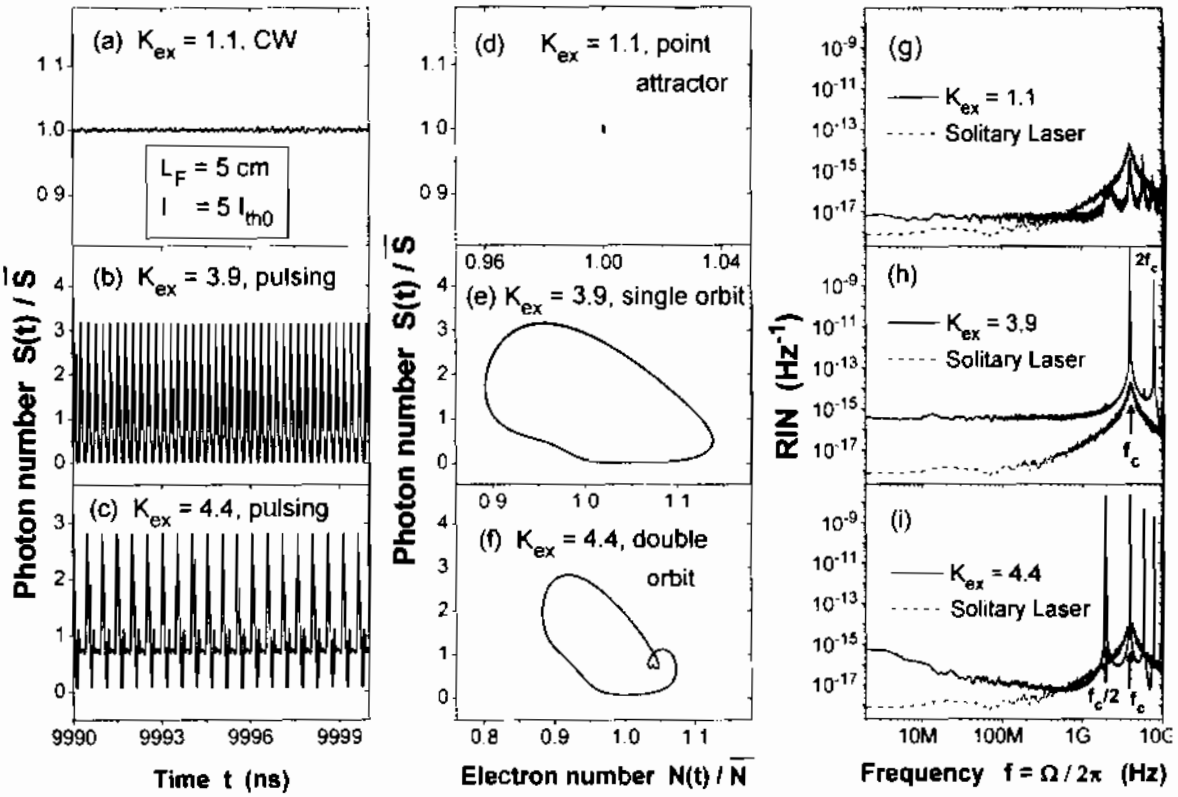

Fig. (3). The simulated data of (a)-(e) time variation of the photon number $S(t)$, (d)-(f) phase portraits, and (g)-(i) RIN spectra when K_{ex}=1.1, 3.9 and 4.4, respectively.

Figure 3(b) indicates that the laser emits regular pulses when K_{ex}=3.9, although the device is injected with a DC current. The phase portrait 3(c) indicates an attractor of a single orbit, which characterizes the regular pulsation. However such attractor deviates from the perfect case of the limit cycle attractor because the pulses are broadened and have

tails in their lower side. The RIN spectrum in Fig. 3(h) exhibits very high and sharp peak around f_c, and the low-frequeney part of the RIN is almost flat (white noise) but is 2.5 orders of magnitude higher than the eorresponding level of the solitary laser. This increase of RIN is beeause of the deviation of the limit attractor from the circular type.

Figure 3(c) shows another type of pulsation induced by the strong OFB (K_{ex}=4.4); the pulsation is period doubling, where the pulses have two distingnished peaks; the frequency of each pulsation is the sub-harmonie $f_c/2$, while the fine freqnency is f_c itself. The phase portrait in Fig. 3(f) reflects this result with the double-orbit attraetor. The RIN spectrum in Fig. 3(i) exhibits very high and sharp peaks around the sub-harmonic $f_c/2$ and its higher harmonics. Although the low frequency part is as high as the case of K_{ex}=3.9, it behaves as a $1/f$ dependency.

4.2. Effects of OFB and the external cavity length on the laser output

Influence of the OFB on the laser output is discussed in terms of the bifureation diagram shown in Fig. 4, which is a convenient method for showing the type of route to chaos of the laser (Mork *et al.*, 1992). The diagram is calculated numerically at a constant current of $5I_{th0}$, and is eonstrueted by picking up the peak(s) $S_{peak}(t)$ of the time-varying photon number $S(t)$ normalized by the corresponding time-averagc value $\bar{S}$ at each strength K_{ex} of OFB. Figure 4(a) plots the obtained diagram when L_F=5 cm. For small values of K_{ex}, the laser still operates stably in CW; the figure plots points that represent weak fluetuations of $S(t)$ around $\bar{S}$. At a certain value of K_{ex}=0.03, the laser output becomes periodic as the relaxation oscillations become undampled. The result is then a single point in the bifurcation diagram (or several adjacent points tbat represents fluctuation components on the pulses due to inclusion of the Langevin noise sources). At another critical value of K_{ex}=0.07, the laser begins a period-doubling route to chaos. Such chaotic operation induces strong instabilitics in the laser operation and enhances the laser noise (Ahmed *et al.*, 2004). The chaos disappears abruptly when K_{ex}~0.11, giving a way to a region of CW-operation followed by a region of frequency locking in which the output is once again stable and periodic. At K_{ex}=0.31 and 2.8, the laser enters also other two regions of pulsing operation interrupted by a window of CW operation. The rangc of OFB over which the regular pulsation extends decreases and the pulses becomc almost period-doubling with the increase of K_{ex}. It is interesting to note that the locking frequency of each pulsing cycle increases with thc increase of K_{ex}, starting with the laser relaxation frcquency f_r in the first cyclc, passing through the compound-cavity mode-frcquency separation f_c, and ending with the external-cavity mode-frequency separation f_{ex}.

We also analyze thc effect of thc length of the external cavity L_F on thc laser cavity. Figures 4(b)-(d) plot the diagrams for longer cavities L_{ex}=10, 30 and 100 cm, respectivcly. When L_F=10 cm, the figure shows two chaos cycles separated by a CW region. The laser still exhibits a region of frcquency locking in the strong OFB regime but at K_{ex} values larger than the case of L_F=5 cm. In the case of L_F=30 cm, Fig. 4(c) shows that the chaos cycles bccomc wider. The route-tochaos of the first cycle is still periodic, whereas it is quasi-periodic in the second cycle. Morcovcr, the pulses in thc frequency locking regime of strong OFB bccomes period doubling or tripling, which degrades thc laser stability and promotes the RIN level. Figure 4(d) indicates much wider two chaos cycles (i.e., more unstable operation) with both cycles having quasi-period routes-tochaos. The pulses in the strong OFB regime become more irregular.

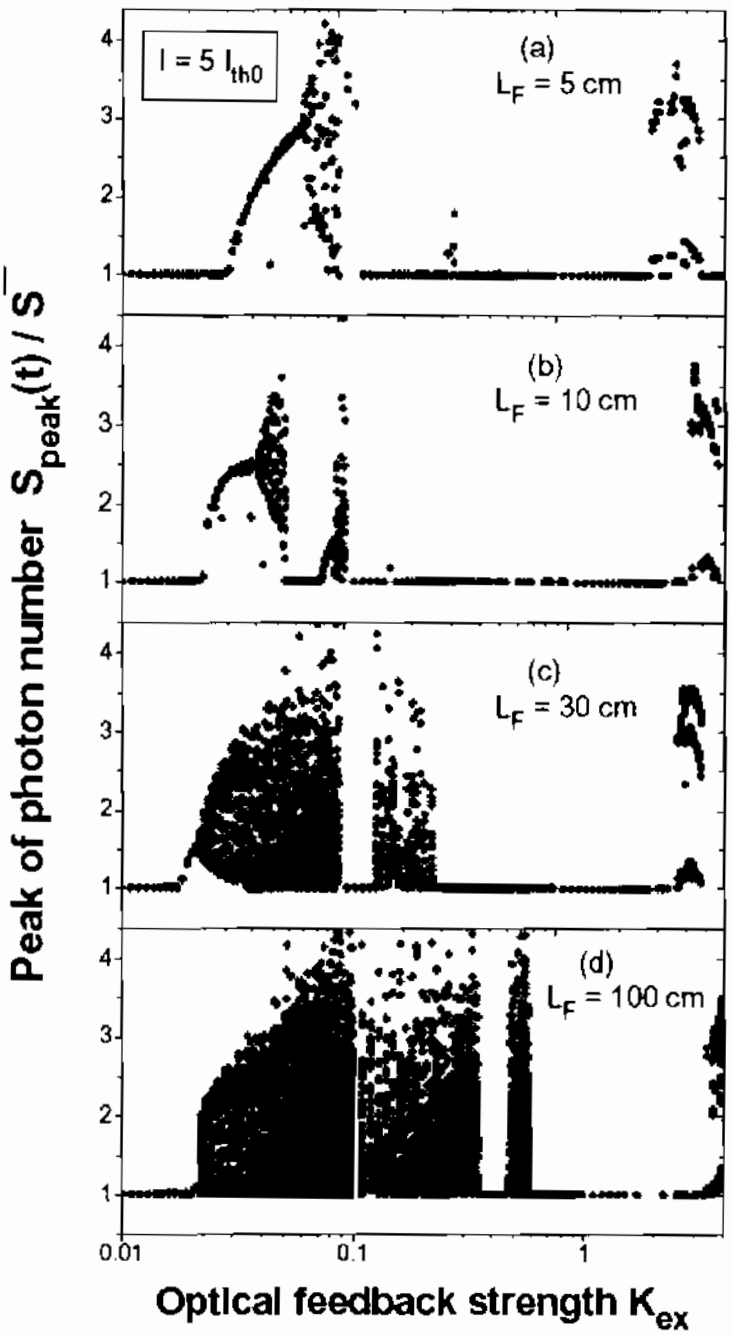

Fig. (4). Bifurcation diagrams of the laser photon number $S(t)$ under external cavity of length (a) L_F=5 cm, (b) L_F=10 cm, (c) L_F=30 cm, and (d) L_F=100 cm. The operation is almost pulsing or CW under shorter cavity. The instabilities increase and the operation becomes more chaotic with the increase of L_F.

4.3. Effect of OFB on the output power

The power emitted from the fiber grating P_g, i.e., the pumping power of the fiber amplifier, is an important parameter of the optical fiber amplifier system. The power P_g is calculated based on a traveling wave model of the lasing field in the laser and external cavities (Abdulrhmann *et al.*, 2003),

$$P_g(t)=\frac{\hbar\omega c}{2n_{r2}L}\frac{n_F}{n_D}(1-R_g)(1-R_f)\frac{(1/2)\ln(1/R_fR_b)+\ln(1/|U|)}{1+\left[1/\sqrt{R_b}-\sqrt{R_b}\right]\sqrt{R_f}|U|-|U|^2R_f}|X|^2S(t) \quad (20)$$

where X is another OFB function describing transmission of the lasing field in the external cavity, and is given by.

$$X=1+\sqrt{R_gR_f}\,e^{-j\omega\tau}\sqrt{\frac{S(t-\tau)}{S(t)}}e^{j[\theta(t-\tau)-\theta(t)]} \quad (21)$$

Figure 5 plots variation of the time-averaged power $\bar{P}_g$ with the variation of the feedback strength K_{ex} when L_F=5 cm and I=5I_{th0}. The figure shows that $\bar{P}_g$ increases monotonically with K_{ex} until K_{ex}~1, then it increase rapidly. This result explains the reason why AR-coating and high-reflectivity gratings (i.e., very weak R_f, very strong R_g, and very large K_{ex}) are desirable in the design of pumping lasers and optical fiber grating systems.

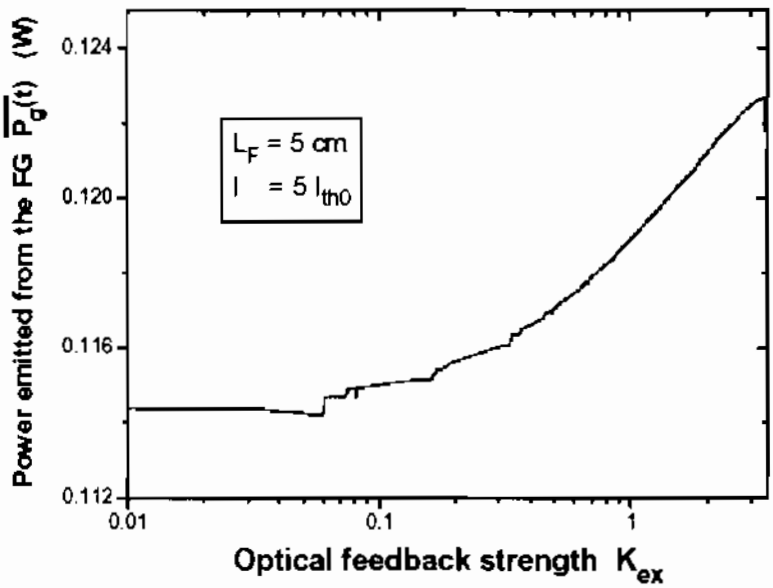

Fig. (5). Variation of the power emitted from the FG with the strength K_{ex} of the OFB. The power increases slowly under low OFB but rapidly under strong OFB.

5. Conclusion

We characterized the influence of OFB on the operation stability and noise of semiconductor lasers in optical fiber communication systems. The study is based on an improved time-delay model. The following conclusions can be drawn.

1- The operation is almost periodic with frequency locking at the compound-cavity modeseparation frequency or the external-cavity mode-separation frequency under strong external optical feedback.

2- When the external cavity is short, the operation is almost stable and is either pulsing or continuous wave. The low-frequency part of the relative intensity noise is lowest under continuous wave. The low-frequency noise is flat when the pulsation is uniform, but decreases as 1/*f* when the pulsation is period doubling or tripling.

3- The instabilities increase and the noise level increases with the inerease of the length of the external cavity. The operation is almost chaotie separated by narrow regions of continuouswave operation.

Aeknowledgements

The authors would like to thank Prof. Minoru Yamada at Kanazawa University, Japan for discussion.

Referenees

[1] **Abdulrhmann Salah, Ahmed Moustafa,** and **Yamada Minorn,** (a) "New model of analysis of semiconduetor laser dynamics under strong optical feedback in fiber communication systems", *SPIE*, **vol. 4986,** pp. 490-501, 2003, (b) "Analysis of dynamies and intensity noise of semiconductor lasers under strong optical feedback", *Inst. Phys. Conf. Series*, **vol. 147:** *Compound Semiconductors 2002,* pp. 409-413, (2003).

[2] **Abdulrhmann Salah, Ahmed Moustafa, Takaharu. Okamoto, Wataro Ishimori,** and **Yamada Minoru,** "An improved analysis of semiconductor laser dynamics under strong optical feedback," *IEEE Journal of Selected Topics in Quantum Electronics*, **vol. 9,** (2003), in Press.

[3] **Agrawal Govind. P.,** *Optical Fiber Communication Systems*, Van Nostrand Reinhold, New Yourk, (2003).

[4] **Ahmed Moustafa** and **Yamada Minoru,** (a) "An infinite order perturbation approach to gain calculation in injection semiconductor lasers", *Journal of Applied Physics*, **vol. 84,** No. 6, 3004- 3015, (1998), (b) "A theoretical study on the perturbation expanded higher order nonlinear gain coefficients in injection semiconductor lasers", *SPIE*, **vol. 3283,** pp. 485-496, (1998).

[5] **Ahmed Moustafa, Yamada Minoru,** and **Saito Masayuki,** "Numerical modeling of intensity and phase noises in semiconductor lasers", *IEEE Journal of Quantum Electron.,* **vol. 37,** pp. 1600- 1610, (2001).

[6] **Ahmed Moustafa,** "Numerical characterization of intensity and frequency fluctuations associated with mode hopping and single-mode jittering in semiconductor lasers", *Physica D*, **vol. 176,** pp. 212-236, (2003).

[7] **Ahmed Moustafa, Abdulrhmann Salah,** and **Yamada Minoru,** "Optical feedback-induced noise in laser diodes in optical-disc systems", *Proceedings of the 46th IEEE Midwest Symposium on Circuits and Systems (MWSCAS'2003)*, Cairo, in Press, (2004).

[8] **Mukai T.** and **Otsuka K.,** "New route to optical chaos: Suceessive-Subharmonic-Oscillation Cascade in a semiconductor laser coupled to an external cavity," *Phys. Rev. Lett.,* **vol. 55,** pp.1711-1714, (1985).

[9] **Press W.H., Teukolsky S.A., Vetterling W.T.,** and **Flannery B.P.,** *Numerical Recipes in Fortran: The art of scientific computing* (Cambridge Univ. Press, New York, 1992).

[10] **Mork J., Tomborg B.,** and **Mark J.,** "Chaos in semiconductor laser sixth optical feedback: theory and experiment," *IEEE J. Quantum Electron.,* **vol. 28,** pp. 93-108, (1992).

استقرار عمل ليزر أشباه الموصلات فى أنظمة اتصالات الألياف الضوئية

مصطفى فرغل أحمد وصفوت وليم زكى محمود

قسم الفيزياء ، كلية العلوم ، جامعة المنيا – جمهورية مصر العربية

المستخلص. يتم حديثاً استخدام مكبرات الألياف الضوئية لتعويض الضعف الذي تعانيه الإشارة الضوئية نتيجة إرسالها خلال الألياف الضوئية فى أنظمة الاتصالات الضوئية مما يسهم فى زيادة مسافة الاتصال. ويتم فى هذه الأنظمة استخدام ليزر أشباه موصلات ذى فتحة أمامية مطلاه بمادة ذات انعكاس ضوئي منخفض كمصدر للضخ، كما يتم استخدام محزوز ألياف للتحكم فى الطول الموجى للإشارة المرسلة. ونتيجة لذلك فإن الليزر يتعرض لتغذية ضوئية عكسية مما قد يتسبب فى عدم استقرار عمل الليزر وارتفاع مستوى ضوضاء شدة الضوء مما يضعف من مصداقية وكفاءة أنظمة الاتصالات.

وفى هذا البحث نقوم بتحليل ديناميكية واستقرار عمل الليزر المستخدم فى ضخ أنظمة مكبرات الألياف الضوئية بغرض اكتشاف مناطق تشغيل الليزر المستقرة والتى تتميز بمستوى منخفض لضوضاء الشدة. وتعتمد هذه الدراسة على نموذج زمنى تأخرى لمعادلات التغير الآنى لعدد الفوتونات والتغير فى الطور الضوئى وعدد الإلكترونات المحفونة. وتتم التحليلات النظرية فى هذا البحث بدلالة التشتتات الآنية لشدة الضوء المنبعث وكذلك المنحنيات الطيفية للضوضاء النسبية لها. ونقوم فى هذا البحث بتصنيف منحنيات ضوضاء الشدة فى مناطق التشغيل المستقرة وغير المستقرة، ونستعرض التحليلات النظرية لمسافات مختلفة للتجويف الرنينى الخارجى المتكون بين الفتحة الأمامية لليزر ومحزوز الألياف.

الاستنتاجات المستخلصة:

١- يكون التغير الآنى لعدد الفوتونات على شكل إشارات منتظمة فى حالة التغذية العكسية القوية (عندما يكون معامل التغذية العكسية K_{ex} مساوياً 4.4) وتيار الحقن خمسة أضعاف قيمته عند عتبة الليزر وطول التجويف الخارجى L_{ex} مساوياً 5 سم.

٢- المنحنى الطيفى المناظر للضوضاء النسبية يتميز بقمم عالية الشدة عند التردد المناظر للتجويف الخارجى f_{ex} ومضاعفاته بعكس المنحنى المميز للّيزر المنعزل الذى يظهر قمة واحدة عند تردد الاسترخاء المميز للتجويف الداخلى للّيزر.

٣- تعنى هذه النتائج أن اهتزاز ضوء الليزر يثبّت عند التردد f_{ex}. وأن التغذية العكسية تتسبب فى رفع مستوى الضوضاء بقيمة رتبتين تقريباً.